INSTITUTE OF PHYSICS PUBLISHING SUPERCONDUCTOR SCIENCE AND TECHNOLOGY
Supercond. Sci. Technol. **16** (2003) 1097–1108 PII: S0953-2048(03)62224-4

A scaling law for the critical current density of weakly- and strongly-coupled superconductors, used to parameterize data from a technological Nb_3Sn strand

Simon A Keys and Damian P Hampshire

Department of Physics, Superconductivity Group, University of Durham, South Road, Durham DH1 3LE, UK

E-mail: d.p.hampshire@durham.ac.uk

Received 8 April 2003, in final form 7 July 2003
Published 14 August 2003
Online at stacks.iop.org/SUST/16/1097

Abstract

There is currently no consensus on how best to parameterize the large volume of data produced in measuring the magnetic field (B), temperature (T) and strain (ε) dependence of the engineering critical current density ($J_E(B, T, \varepsilon)$) for A15 superconducting strands. For the volume pinning force (F_P) and the upper critical field $B_{C2}(T, \varepsilon)$, we propose

$$F_P = J_E(B, T, \varepsilon) \times B = \alpha(\varepsilon)[T_C(\varepsilon)(1 - t^2)]^2 \times \frac{[B_{C2}(T, \varepsilon)]^{n-2}}{(2\pi\Phi_0)^{1/2}\mu_0} b^p(1 - b)^q \quad \text{and} \quad B_{C2}(T, \varepsilon) = B_{C2}(0, \varepsilon)[1 - t^v]$$

given $b = B/B_{C2}(T, \varepsilon)$ and $t = T/T_C(\varepsilon)$ where $T_C(\varepsilon)$ is the critical temperature. F_P (or $J_E(B, T, \varepsilon)$) includes three strain-dependent variables $\alpha(\varepsilon)$, $B_{C2}(0, \varepsilon)$ and $T_C(\varepsilon)$ and four constants, n, p, q and v. The form is different to that proposed by Summers *et al* by a factor $T_C^2(\varepsilon)$. We suggest that the form is sufficiently general to describe superconductors whether the electron–phonon coupling is weak or strong and find that $\alpha(\varepsilon)$ is proportional to

$$\frac{\mu_0\gamma(\varepsilon)}{\left[1 - \frac{1}{5}\left(\frac{2\Delta(\varepsilon)}{k_B T_C(\varepsilon)} - 3.53\right)\right]}$$

where $\Delta(\varepsilon)$ is the superconducting gap and $\gamma(\varepsilon)$ is the Sommerfeld constant. Comprehensive $J_E(B, T, \varepsilon)$ data are presented for a modified jelly-roll (MJR) Nb_3Sn conductor that are consistent with the form proposed with $n \approx \frac{5}{2}$, $p = \frac{1}{2}$, $q = 2$ and $v = 1.374$. Hence the scaling law proposed leads to a critical current density for the MJR Nb_3Sn given by

$$J_E(B, T, \varepsilon) \approx \frac{\alpha(\varepsilon)}{(2\pi\Phi_0)^{1/2}\mu_0}[T_C(\varepsilon)(1 - t^2)]^2 B_{C2}^{-1/2}(T, \varepsilon) b^{-1/2}(1 - b)^2.$$

Comparison with data in the literature suggests that $\alpha(\varepsilon) \approx 3 \times 10^{-3}\mu_0\gamma(\varepsilon)$. Furthermore, the volume pinning force ($F_{P(S/C)}$) within the Nb_3Sn superconducting filaments alone can be described in terms of

superconducting parameters in the form

$$F_{P(S/C)} \approx \frac{1}{100} \frac{B_{C2}^{5/2}(T, \varepsilon)}{(2\pi \Phi_0)^{1/2} \mu_0 \kappa^2(T, \varepsilon)} b^{1/2}(1-b)^2$$

where $\kappa(T, \varepsilon)$ is the Ginzburg–Landau parameter.

1. Introduction

Scaling laws have proved useful for describing the magnetic field and temperature dependence of the engineering critical current density (J_E) of superconductors for more than 30 years [1, 2]. Theoretical work [3, 4] and experimental data [5–10] have helped encapsulate the concept of pinning sites and contributed to improved processing of superconducting materials. With the development of large superconducting magnet systems, the effects of strain and irradiation damage on some superconducting properties have been measured and attempts made to include them in the scaling laws [5, 6, 8, 11]. The original measurements, by Fietz and Webb [1], of the field and temperature dependence of $J_E(B, T)$ were parameterized in terms of a volume pinning force (F_P). Subsequently, the effect of strain was measured, most notably the comprehensive $J_E(B, \varepsilon)$ measurements at 4.2 K by Ekin, and parameterized using a scaling law of the Fietz–Webb type [5, 6]. A somewhat different approach by Hampshire *et al* parameterized comprehensive $J_E(B, T)$ data for Ta doped Nb_3Sn [7] by including the temperature dependence of the Ginzburg–Landau parameter (κ). Summers *et al* found empirical forms for B_{C2} and κ and endeavoured to unify the scaling laws for $J_E(B, T)$ data and $J_E(B, \varepsilon)$ data with a view to describing the effect of irradiation damage on J_E [8, 11]. Summers' formulism was developed before comprehensive variable strain $J_E(B, T, \varepsilon)$ measurements at temperatures other than 4.2 K were available and slightly modified versions are probably the most widely used now to parameterize large data sets [12, 13]. Measurements on bronze-route Nb_3Sn that were analysed within the Fietz–Webb framework have shown that $J_E(B, T)$ data at fixed strain gives a different scaling law to that found from $J_E(B, \varepsilon)$ data at fixed temperature [14, 15]. This inconsistency implies a physical interpretation of the free parameters obtained using a standard Fietz–Webb scaling law (i.e. without $\kappa(T, \varepsilon)$) is questionable so that at best the free parameters provide an empirical parameterization. Recently, the authors of this current paper have published comprehensive $J_E(B, T, \varepsilon)$ data for a technological Nb_3Al [16] strand which provided a unified scaling law that describes strain and temperature scaling and is consistent with the $J_E(B, T)$ data for bronze-route $(Nb, Ta)_3Sn$ [7]. The inconsistencies between parameterization of variable-temperature and variable-strain data [14] were resolved by extending earlier work to incorporate the strain as well as the temperature dependence of $\kappa(T, \varepsilon)$ within the Ginzburg–Landau framework [17] and microscopic theory [18]. The current paper uses the unified scaling law to describe new comprehensive $J_E(B, T, \varepsilon)$ data on a modified jelly-roll (MJR) Nb_3Sn strand. It is shown that the form of the scaling law can be justified in both the weak and strong-coupling limits. The scaling law includes a physical interpretation for the strain-dependent free parameters so one can expect it to aid in describing the effect of radiation damage on J_E as more such data become available.

Furthermore, regardless of how much (or even whether) the scaling laws are properly understood, the engineering community has continued developing superconducting magnets for cryocooled systems, particle accelerators and Tokamaks [19]. Our group has put significant effort into obtaining comprehensive $J_E(B, T, \varepsilon)$ data for a range of A15 superconducting strands [14–16, 20–22]. These data are required to model and optimize the design of magnet systems. Since to our knowledge, there is no consensus on how best to parameterize such data [11, 23], a scaling law (or at least some agreed mathematical framework) is required: to accurately describe $J_E(B, T, \varepsilon)$; to avoid introducing errors that can occur when transferring or analysing large amounts of data; to facilitate comparison of data from different experimental groups over a range of parameter space rather than simply at a single magnetic field or strain as at present and to aid improvement in modelling the properties of developmental high field superconducting strands. This paper uses the unified scaling law to parameterize the new data for MJR Nb_3Sn, provides a comparison with equivalent results for Nb_3Al and compares the law to that of Summers *et al*.

2. Experimental details

The strands examined in this work were 0.5 mm diameter modified jelly-roll Nb_3Sn with niobium diffusion barriers [24]. The preparation of the samples and the subsequent variable temperature measurements broadly followed the methods described in previous reports on the effect of hot isostatic pressing on the strain tolerance of these wires at 4.2 K and of comprehensive $J_E(B, T, \varepsilon)$ measurements on Nb_3Al [16, 21].

Two nominally identical samples were reacted together on oxidized stainless-steel reaction mandrels under argon using the manufacturers recommended heat-treatment: 210 °C for 100 h followed by 340 °C for 48 h and finally 650 °C for 180 h. Each sample was then carefully transferred onto a dedicated Cu–Be spring and soldered to it. Four-terminal critical current and resistivity measurements were made [25]. Strand 1 was measured directly immersed in liquid helium at 4.2 K in the strain range $-2.15\% \leqslant \varepsilon \leqslant 0.45\%$. Strand 2 was measured at temperatures above 4.2 K in the range 4.2 K $< T \leqslant 20$ K for strains of $-1.6\% \leqslant \varepsilon \leqslant 0.45\%$. Both strands were measured in fields up to 15 T.

The apparatus has been described in detail elsewhere [16, 20]. During the critical current measurements, the current flow direction ensured that the Lorentz force produced on the wire in-field pushed the strand into the spring. Both tensile

and compressive strain were applied to the strand by twisting one end of the spring with respect to the other [26]. In these measurements, the spring is inside an isolated enclosure and surrounded by a single heater which was used in a feed-back loop with a Cernox control thermometer to set and control the temperature of the strand during the measurements [27, 28]. The Cernox thermometer was calibrated commercially in zero field and the (small) in-field correction measured in-house and accounted for in setting the temperature [16]. The Cernox was mounted directly next to the section of the strand measured.

The procedure to take the measurements was as follows: the strain was set to the value required. Measurements were made of the critical current (I_C) as a function of field at all the temperatures required. For strand 2, measurements of the magneto-resistance of the wire and shunt were then made above B_{C2} (i.e. in the normal state) in the range 5–20 K. I_C was recorded at a criterion of 10 μV m^{-1}. Resistivity measurements were then made at fixed fields from 0 to 15 T every 3 T as a function of temperature. The measurements were made using a lock-in amplifier operating at 76 Hz. Data were obtained at two different excitation currents: 82 mA and 28 mA. The strain was then set to the next required value by twisting the spring and the series of in-field measurements repeated until all the data were obtained. All currents quoted in this paper have had the magnetic-field and strain-dependent current that flows in the shunt (approximately 13 mA at 10 μV m^{-1}) subtracted from the total current in order to calculate I_C for the superconductor alone. Critical current density (J_C) and the engineering critical current density (J_E) are both widely and interchangeably used in the literature. This paper uses J_E which is defined as the critical current (I_C) for the strand divided by the entire cross-sectional area of the strand. J_E is the useful engineering parameter although it ignores the fact that the supercurrent is predominantly confined to the superconducting cross-sectional area of the composite. Furthermore, the units for strain are expressed throughout in per cent (%) which again is most commonly used amongst the engineering and magnet technology community. Unfortunately, using natural or dimensionless units introduces a series of very small numbers for the magnitude of the applied strain and very large numbers required to describe strain dependencies of the critical parameters which together mitigate against accurate parameterization.

3. Scaling law for $J_E(B, T, \varepsilon)$ data

The basic equation that describes the scaling of the critical current density includes the volume pinning force (F_P) and is given by

$$F_P = J_E \times B = Cb^p(1-b)^q \tag{1}$$

where b is the reduced field (B/B_{C2}), and p and q are constants. Fietz and Webb first proposed this equation to describe the magnetic field and temperature dependence of F_P. It describes the data for many low-temperature type-II superconductors [1, 4, 29, 30]. They proposed that the prefactor was given by

$$C = AB_{C2}^n \tag{2}$$

where A and n are constants. However, in order to describe the effect of strain on the critical current density accurately (and unify the strain and temperature scaling laws [14]), the parameter A must be made a function of strain [5, 14, 31]:

$$F_P = J_E \times B = A(\varepsilon)B_{C2}^n(T, \varepsilon)b^p(1-b)^q. \tag{3}$$

For low-temperature A15 conductors, the upper critical field data can be parameterized using the empirical equation [32, 33]:

$$B_{C2}(T, \varepsilon) = B_{C2}(0, \varepsilon)[1 - t^v] \tag{4}$$

where $t = T/T_C(\varepsilon)$. $B_{C2}(0, \varepsilon)$ and $T_C(\varepsilon)$ are the strain-dependent upper critical field at 0 K and the critical temperature respectively and v is a constant. Hence to parameterize F_P (or $J_E(B, T, \varepsilon)$), there are three strain-dependent variables $A(\varepsilon)$, $B_{C2}(0, \varepsilon)$ and $T_C(\varepsilon)$ and four constants, n, p, q and v.

One can also consider a scaling law of the form which explicitly includes the Ginzburg–Landau parameter ($\kappa(T, \varepsilon)$) [7, 16]:

$$F_P = A^*(\varepsilon)\frac{[B_{C2}(T, \varepsilon)]^n}{(2\pi\Phi_0)^{1/2}\mu_0[\kappa(T, \varepsilon)]^m}b^p(1-b)^q \tag{5}$$

where $A^*(\varepsilon)$ is a function of strain alone. Previous work utilized an expression for κ in the weak-coupling limit [7, 16]. In this work, we consider the effect of strong-coupling terms on κ. In order to accurately derive the relevant generalized BCS relations to include strong coupling, numerical solutions of the complete Eliashberg equations are required [18]. Approximate expressions have been derived in the literature using the strong- coupling variable T_C/ω_{ln}, where ω_{ln} is the Allen–Dynes expression for the average phonon energy [34, 35]. However, we consider describing the strong-coupling corrections in terms of the BCS ratio $2\Delta/k_BT_C$ which has the value 3.5 for weak coupling [18] and is higher when materials are strongly coupled (e.g. Al $\sim$ 3.5, Nb $\sim$ 3.9, Nb_3Sn and Nb_3Al $\sim$ 4.6) [35]. Following the spirit of the work by Moore *et al* [36], we describe the Eliashberg solutions by linear equations using the data from Marsiglio and Carbotte [35] and suggest that the BCS relations in the strong-coupling limit can be reasonably approximated by

$$\frac{2\Delta}{k_BT_C} = 3.53 + 7.35\frac{T_C}{\omega_{ln}} \tag{6}$$

and

$$\frac{\mu_0\gamma T_C^2}{B_C^2(0)} = 2.11 - 3.10\frac{T_C}{\omega_{ln}} \tag{7}$$

where γ is the Sommerfeld constant. Rearranging, we find

$$B_C(0) = \frac{0.69\mu_0^{1/2}\gamma^{1/2}T_C}{\left[1 - \frac{1}{5}\left(\frac{2\Delta}{k_BT_C} - 3.53\right)\right]^{1/2}} \tag{8}$$

where the denominator is the strong-coupling correction [37]. Using the two-fluid model for the temperature dependence $B_C(T, \varepsilon) = B_C(0, \varepsilon)[1 - t^2]$ and the Ginzburg–Landau relation for the upper critical field $B_{C2}(T, \varepsilon) = \sqrt{2}\kappa(T, \varepsilon)B_C(T, \varepsilon)$ [17, 38], an empirical relation for κ which includes strong-coupling corrections is found of the form

$$\kappa(T, \varepsilon) = \frac{B_{C2}(T, \varepsilon)}{\sqrt{2}B_C(T, \varepsilon)} = 1.03\frac{B_{C2}(T, \varepsilon)}{\mu_0^{1/2}\gamma^{1/2}(\varepsilon)T_C(\varepsilon)[1 - t^2]} \times \left[1 - \frac{1}{5}\left(\frac{2\Delta}{k_BT_C} - 3.53\right)\right]^{1/2}. \tag{9}$$

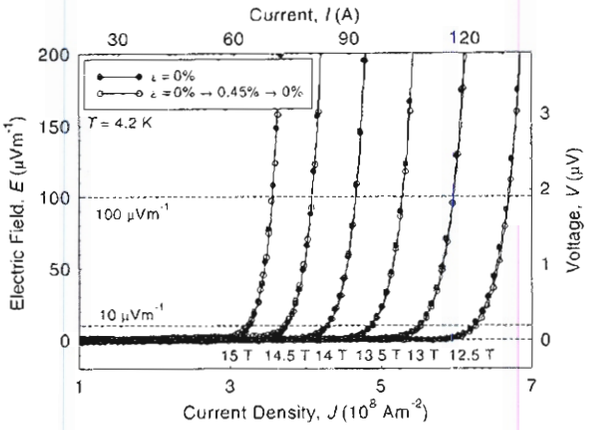

Figure 1. Electric field–current density characteristics for zero applied strain at 4.2 K for the Nb_3Sn strand. The data demonstrate that, independent of criterion, J_E is reversible. The strain was cycled as detailed in the legend.

Substituting into equation (5) gives

$$F_P = \alpha(\varepsilon)[T_C(\varepsilon)(1-t^2)]^m \frac{[B_{C2}(T,\varepsilon)]^{n-m}}{(2\pi\Phi_0)^{1/2}\mu_0} b^p (1-b)^q \quad (10)$$

where

$$\alpha(\varepsilon) = A^*(\varepsilon)\left[\frac{\mu_0\gamma(\varepsilon)}{1.06\left[1-\frac{1}{5}\left(\frac{2\Delta}{k_B T_C}-3.53\right)\right]}\right]^{\frac{m}{2}}. \quad (11)$$

It is worth noting that were the non-linearized forms for the BCS relations in the strong- coupling limit used, it would not affect the form of equation (10). Hence in rewriting equation (5) in the form given by equation (10), the main assumptions are that κ in equations (5) and (9) are the same [39], the general validity of the Ginzburg–Landau formulism and the two-fluid form for $B_C(T, \varepsilon)$. In order to understand the focus for this paper, one should also note that although equation (10) is more complex than equation (3), in the context of $J_E(B, T, \varepsilon)$ data, the constant m is the only additional free parameter and that to first order, the strong-coupling correction only affects the strain dependence of $\alpha(\varepsilon)$.

4. Results

4.1. Engineering critical current measurements

Figure 1 shows typical electric field–current density data for strand 1 at 4.2 K and 0% applied strain. Two data sets are shown–measurements taken in the initial state before any strain had been applied (i.e. $\varepsilon = 0\%$) and after a cycle to 0.45% applied tensile strain. Horizontal lines on the figure show the conventional criteria used to define the critical current at 10 and 100 μV m^{-1}. It can be seen that the critical current density is reversible over the strain range shown independent of the criterion used to define it. Figure 2 shows the engineering critical current defined at 10 μV m^{-1} as a function of magnetic field and strain at 4.2 K (strand 1) and 10 K (strand 2). On applying tensile strain, the critical current first increases, reaches a peak and then decreases. The standard interpretation is that the composite

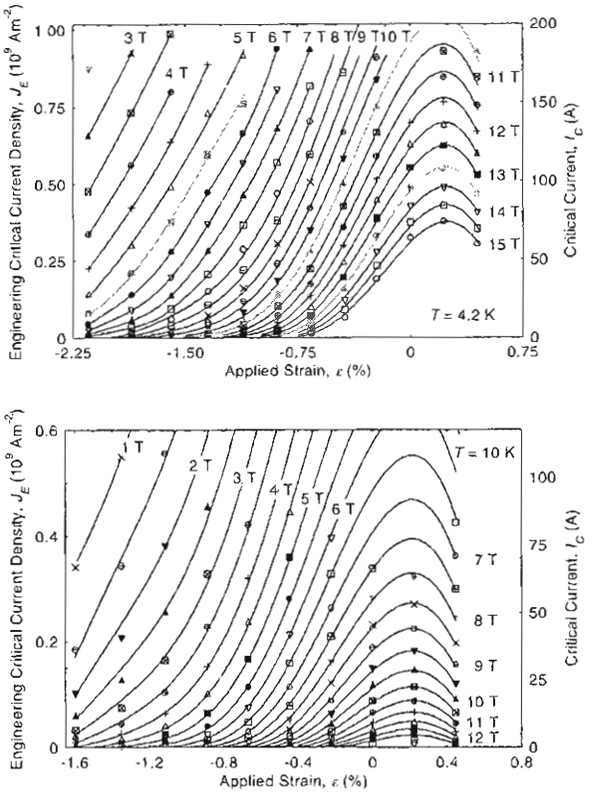

Figure 2. Engineering critical current density at a criterion of 10 μV m^{-1} as a function of applied strain and magnetic field at 4.2 K (upper) and 10 K (lower) for the Nb_3Sn strand. The solid lines are a guide to the eye.

wire puts the superconducting filaments under precompression when cooling down to cryogenic temperatures. The critical current monotonically decreased on applying compression. Hence these comprehensive data sets show similar trends to equivalent data in the literature on other strands [6, 14, 16, 21].

4.2. Resistivity measurements

Figure 3 shows typical resistivity data that can be used to find an estimate of the upper critical field which can be parameterized using equation (4) [32, 33]. If the upper critical field is defined at 5% of the normal state resistivity $\left(B_{C2}^{5\%\rho N}(T,\varepsilon)\right)$ and measured using an excitation current of 28 mA, scaling is observed as shown in figure 4 where $v \sim 1$. A similar value for the exponent v is found whether 50%ρ_N or 95%ρ_N is used to define the upper critical field.

5. Analysis

5.1. The magnetic field dependence

The $J_E(B, T, \varepsilon)$ data were first analysed using the resistivity data to constrain the upper critical field—following the work on Nb_3Al [16]. If the upper critical field is fixed at 5%ρ_N, then over the range of strain measured p varies in the range from 0.2 to 1.25 and q varies from ~2 to 3.5. Larger variations of p and q were found when defining the upper critical field

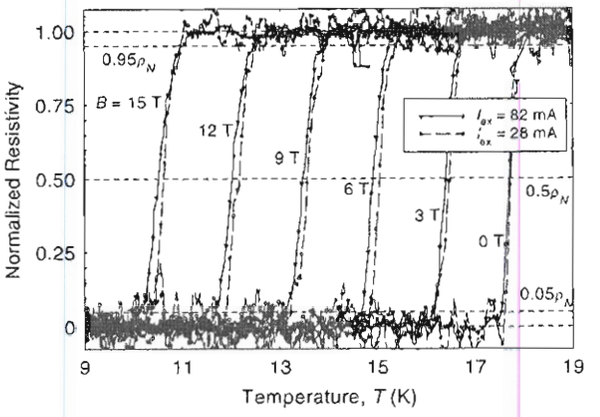

Figure 3. Normalized resistivity as a function of temperature in an applied field of 0, 3, 6, 9, 12 and 15 T at zero applied strain ($\varepsilon = 0\%$) for the Nb_3Sn strand. Data are shown for a current of 28 mA (open) and 82 mA (closed). The horizontal lines show the different criteria used to determine upper critical field.

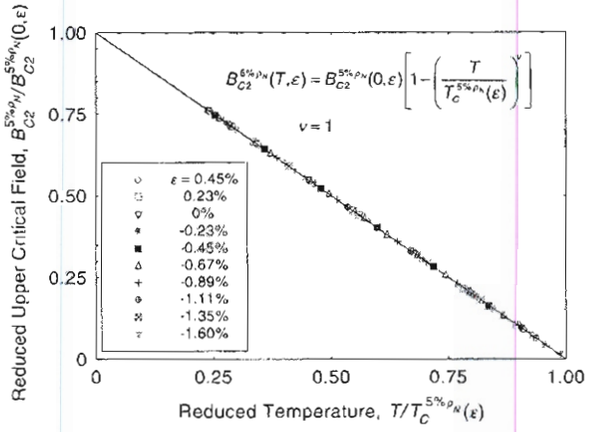

Figure 4. Reduced upper critical field as a function of reduced temperature and applied strain for the Nb_3Sn strand. The upper critical field was determined at 5% of the normal state resistivity.

at $50\%\rho_N$ and $95\%\rho_N$ suggesting that in order to find constant values for p and q (i.e. good F_P scaling), a value of B_{C2} below the resistive transition is required. Hence unlike the Nb_3Al strand [16], there is no clear evidence for F_P scaling using any feature of the resistive measurement of B_{C2}. Indeed, the variations in p and q suggest that the characteristic upper critical field required for good F_P scaling occurs at magnetic fields below the percolation limit. Hence contrary to the expectation that for a homogeneous material, resistivity data give the value for B_{C2}, in this Nb_3Sn MJR inhomogeneous composite the characteristic B_{C2} required for good F_P scaling occurs below the resistivity transition at fields when J_E is not zero. When the value of B_{C2} is set to below the resistivity transition, typical values of q approach 2 which suggests that Kramer values of p and q ($\frac{1}{2}$ and 2 respectively) can provide good fits to the data. Figure 5 shows the $J_E(B, T, \varepsilon)$ versus magnetic field data plotted on Kramer plots at strains of 0.45%, 0%, −0.67% and −1.35% [30, 40]. For critical currents above 5 A, in the technologically important applied strain range $-0.45\% \leqslant \varepsilon \leqslant +0.45\%$, the Kramer functional form fits the data reasonably well—typically with an error less than 1 A. At high compressive strains, the Kramer fits are less good for $I_C < 5$ A—in particular there is a large high-field 'tail'. Of course, not all Nb_3Sn or A15 materials obey the Kramer law [41, 42]. Figure 6 shows the upper critical field $\left(B_{C2}^{\text{Kramer}}(T, \varepsilon)\right)$ derived from the intercept of the Kramer straight lines extrapolated to zero current density. Good scaling of $B_{C2}^{\text{Kramer}}(T, \varepsilon)$ is observed given by equation (4) with $\nu = 1.374$. Comparison between the different temperature dependencies of the scaling law for B_{C2} (i.e. ν) shown in figures 4 and 6 shows how strongly the upper critical field depends on the criterion used to define it. The applied strain dependence of the normalization constants, $B_{C2}^{\text{Kramer}}(0, \varepsilon)$ and $T_C^{\text{Kramer}}(\varepsilon)$ used to obtain the scaling in figure 6 are shown in figure 7. Figure 8 shows that $B_{C2}^{\text{Kramer}}(0, \varepsilon)$ is a linear function of $T_C^{\text{Kramer}}(\varepsilon)$ for both Nb_3Sn presented in this paper and the Nb_3Al measured previously [16]. In conjunction with equation (4) (cf figure 6), these linear equations can be used to find a general temperature-dependent empirical form for $B_{C2}^{\text{Kramer}}(T, \varepsilon)$ in terms of $T_C^{\text{Kramer}}(\varepsilon)$ that leads, for example, at 0 K to $\frac{\partial B_{C2}^{\text{Kramer}}(0,\varepsilon)}{\partial T_C^{\text{Kramer}}(\varepsilon)} = 3.85$ and can be compared to Ekin's relation between the normalized $B_{C2}^*(4.2\text{ K}, \varepsilon)$ and normalized $T_C^*(\varepsilon)$ which can written as $\frac{\partial B_{C2}^*(4.2\text{ K}, \varepsilon \sim \varepsilon_{max})}{\partial T_C^*(\varepsilon \sim \varepsilon_{max})} \cong 3.5$ [6].

5.2. *The temperature and strain dependence*

5.2.1. The exponents n and m. Figure 9 shows the temperature and applied strain-dependent prefactor $C(T, \varepsilon)$ from equation (1). The values of $C(T, \varepsilon)$ are normalized by their maximum value at each temperature and then $\log(C(T, \varepsilon))$ is offset from the preceding temperature by 0.2. The values of $B_{C2}^{\text{Kramer}}(T, \varepsilon)$ are also normalized at each temperature by their maximum value at each temperature. There is very clear curvature in the data in figure 9 which compromises the accuracy of any parameterization using a simple power law of the form given by equation (2). At low temperatures, the gradient of the lines increases by more than a factor 2 as $B_{C2}^{\text{Kramer}}(T, \varepsilon)$ decreases. At the highest values of $B_{C2}^{\text{Kramer}}(T, \varepsilon)$, the gradient of the data at each temperature increases as the temperature increases. Both these features of the data found here for MJR Nb_3Sn were observed for a bronze-route Nb_3Sn wire, such that the exponent for B_{C2} is different (i.e. inconsistent) for variable temperature data at fixed strain and variable strain data at fixed temperature. This led to the parameterization of $C(T, \varepsilon)$ given in equations (3) and (10) [14, 16, 43].

Comparing equation (1) with (10) gives

$$C(T, \varepsilon)\left[\frac{B_{C2}(T, \varepsilon)}{T_C(\varepsilon)(1 - t^2)}\right]^m = \alpha(\varepsilon)\frac{[B_{C2}(T, \varepsilon)]^n}{(2\pi\Phi_0)^{1/2}\mu_0} \qquad (12)$$

In figure 10, $\log C(T, \varepsilon)\left[\frac{B_{C2}(T,\varepsilon)}{T_C(\varepsilon)(1-t^2)}\right]^m$ is plotted versus log $B_{C2}(T, \varepsilon)$ for values of $m = 0$, 2 and 4. For all panels in figure 10, the scatter increases when B_{C2} drops to a few tesla. Despite the scatter, in the low-B_{C2} range there is a clear downward trend in the top panel and a clear upward trend in the bottom panel. The best straight line occurs when $m = 2$ whereas when $m = 0$ the data are concave. This shows that the J_E data are better parameterized by equation (10) than by equation (3). At each strain the data for $m = 2$

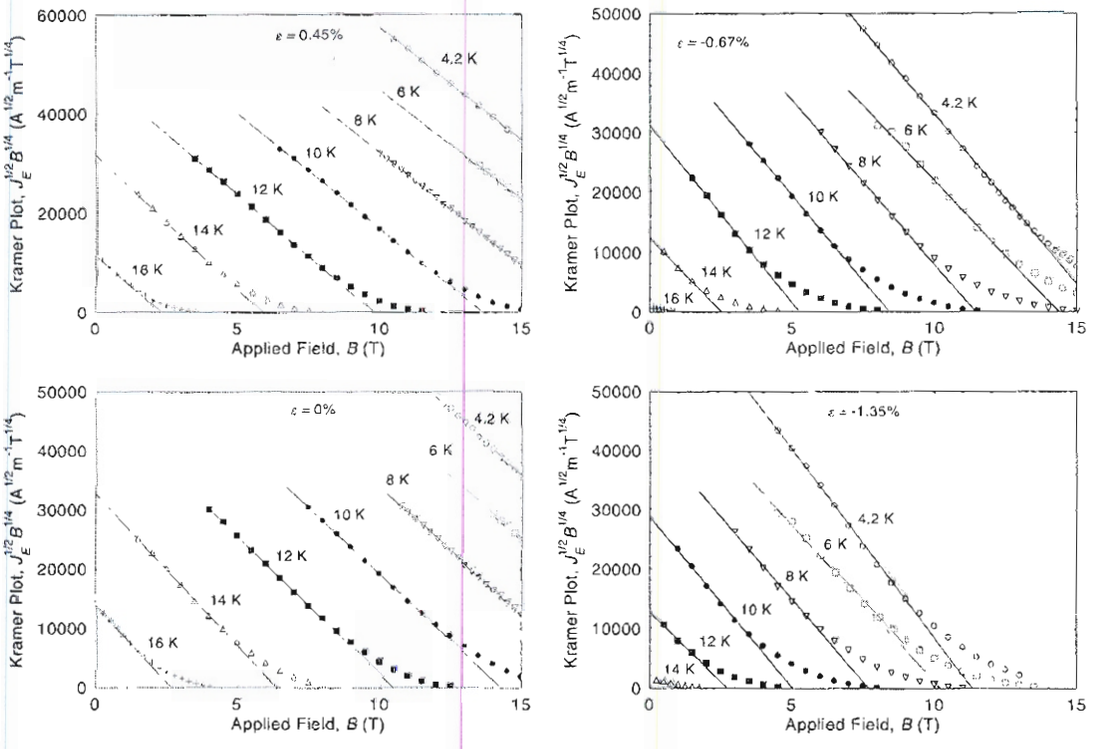

Figure 5. Kramer plots as a function of field and temperature at applied strain values given by $\varepsilon = 0.45\%$, 0%, -0.67% and -1.35% for the Nb_3Sn strand. The solid lines are fits to the data using a Kramer analysis.

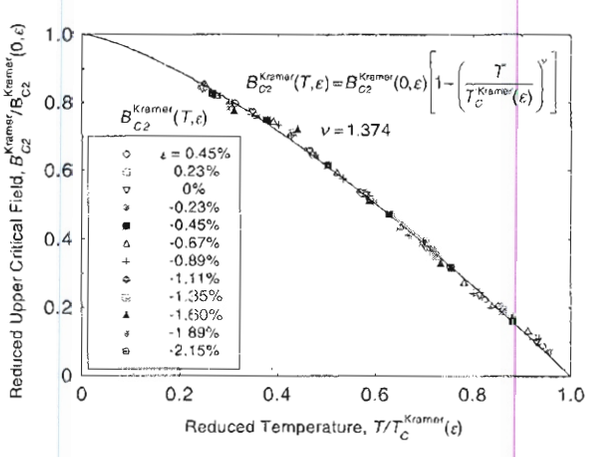

Figure 6. A universal scaling law showing the reduced upper critical field as a function of reduced temperature for a range of different applied strains for the Nb_3Sn strand. The upper critical field was derived from the Kramer analysis.

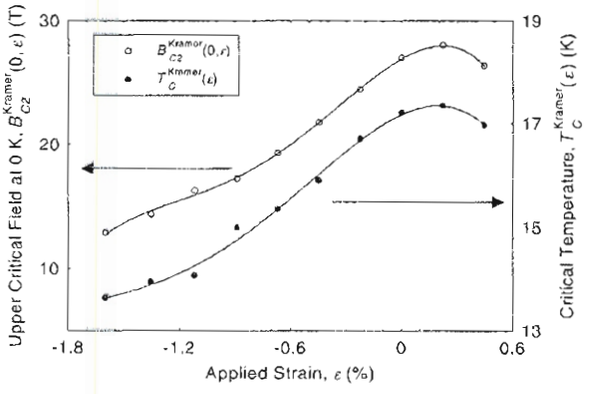

Figure 7. Upper critical field at 0 K and the critical temperature as a function of applied strain for the Nb_3Sn strand derived from the Kramer analysis.

have been fitted by straight lines using least-squares and the gradient and intercept used to determine the exponent n and the value of $\alpha(\varepsilon)$. For the technological range of applied strain $0.45\% \leqslant \varepsilon \leqslant 0.45\%$, $n = 2.53 \pm 0.06$. For the whole strain range (i.e. the entire data set) $n = 2.73 \pm 0.24$. The equivalent numbers for $m = 0$ are 2.36 ± 0.10 and 2.54 ± 0.24 respectively. Figure 10 shows that when parameterizing data limited to a small range of B–T–ε phase space, one may find a relatively large range of values for m that will fit the data equally well—indeed the best value for m will vary depending on the details of the weighting (e.g. whether percentage error, least-squares or absolute differences) for the fit procedure used. Nevertheless, given the results presented here, and that the work on Nb_3Al [16] and $(NbTa)_3Sn$ [7] found that $m \sim 2$, we propose eliminating m as a free parameter by setting $m = 2$ and parameterizing the data using

$$F_P = J_E(B, T, \varepsilon) \times B$$
$$= \alpha(\varepsilon)[T_C(\varepsilon)(1-t^2)]^2 \frac{[B_{C2}(T,\varepsilon)]^{n-2}}{(2\pi\Phi_0)^{1/2}\mu_0} b^p (1-b)^q \qquad (13)$$

where $B_{C2}(T, \varepsilon)$ is given by equation (4). F_P includes three strain-dependent variables $\alpha(\varepsilon)$, $B_{C2}(0, \varepsilon)$ and $T_C(\varepsilon)$ and four

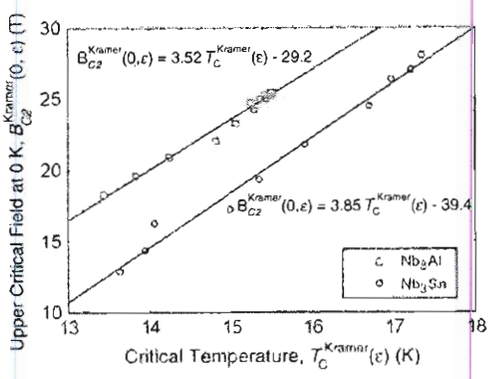

Figure 8. The upper critical field at 0 K versus the critical temperature derived from the Kramer analysis, for different values of strain for the Nb_3Sn strand. Equivalent data for Nb_3Al are also shown that have been calculated using data previously published from our group [16].

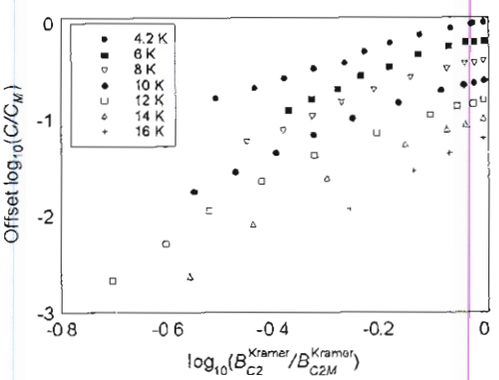

Figure 9. Normalized log–log plot of the scaling law prefactor, C, against upper critical field as a function of applied strain at different temperatures derived from a Kramer analysis of the Nb_3Sn strand. C_M and B_{C2M} are the maximum values for the prefactor and upper critical field respectively. The data at different temperatures have been offset by $\log C = -0.2$.

constants, n, p, q and v. Equation (13) is equivalent to

$$J_E(B, T, \varepsilon) = \alpha(\varepsilon)[T_C(\varepsilon)(1 - t^2)]^2 \times \frac{[B_{C2}(T, \varepsilon)]^{n-3}}{(2\pi\Phi_0)^{1/2}\mu_0} b^{p-1}(1 - b)^q. \quad (14)$$

5.2.2. The strain-dependent variable $\alpha(\varepsilon)$—strong coupling, $2\Delta/k_BT_C$ and the Sommerfeld constant $\gamma(\varepsilon)$. In the seminal work by Dew-Hughes [4], the parameter A^* (equation (5)) is dependent only on the microstructure—independent of temperature, strain and magnetic field. In order to consider whether this is true for the MJR Nb_3Sn presented here, we need to know the strain dependence of $2\Delta/k_BT_C$ and $\gamma(\varepsilon)$. Extensive work by the scientific community to understand both the applied and fundamental properties of Nb_3Sn means that we can start to address these issues, in contrast to say Nb_3Al where data giving the effect of strain on these fundamental properties (in off-stoichiometric material) are sparse. The change in $2\Delta/k_BT_C$ as a function of T_C has been measured in Nb_3Sn films of different tin content which gave

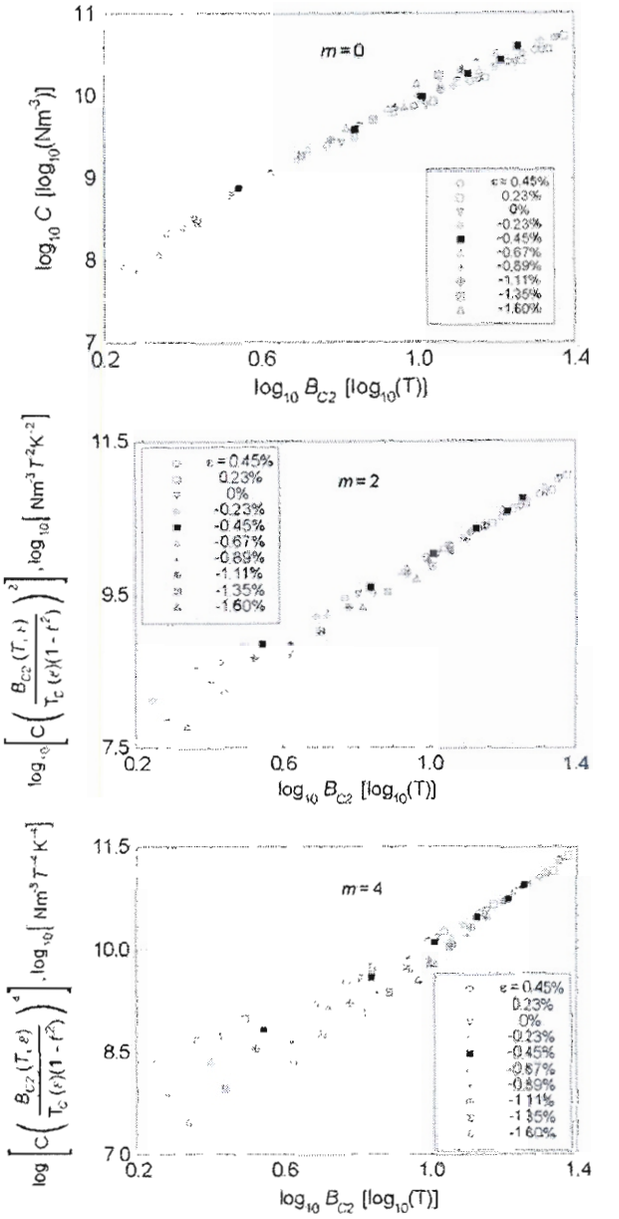

Figure 10. Log–log plot of $C(T, \varepsilon)[\frac{B_{C2}(T,\varepsilon)}{T_C(\varepsilon)(1-t^2)}]^m$ versus the upper critical field generated from the Kramer analysis of the data for the Nb_3Sn strand. Values of $m = 0$ (upper), $m = 2$ (middle) and $m = 4$ (lower panel) have been considered. Note the distinct curvature in the data for the upper and lower panels at low values of B_{C2} in contrast to the good linearity found for the data when $m = 2$.

$2\Delta/k_BT_C = 4.45$ and 3.5 when $T_C = 17.7$ K and 14.4 K respectively [36]. This gives ~20% reduction in the strong-coupling contribution to $\alpha(\varepsilon)$ as T_C drops in compressive strain to −1.6% [36]. However, there are concerns about these measurements because the gap measurements were made using tunnelling but the T_C measurements were made using (bulk) susceptibility which preferentially measures the higher T_C components. Alternatively, using equation (6) for Nb_3Sn and the result $2\Delta/k_BT_C = 4.45$ when $T_C = 17.7$ K implies $\omega_{ln} = 137$ K. If we assume that ω_{ln} only weakly depends

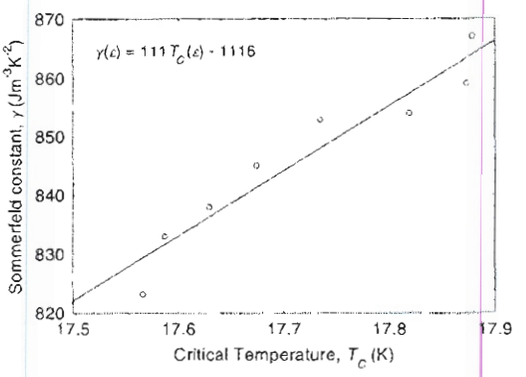

Figure 11. The effect of hydrostatic pressure on the Sommerfeld constant taken from the data from Lim *et al* [45].

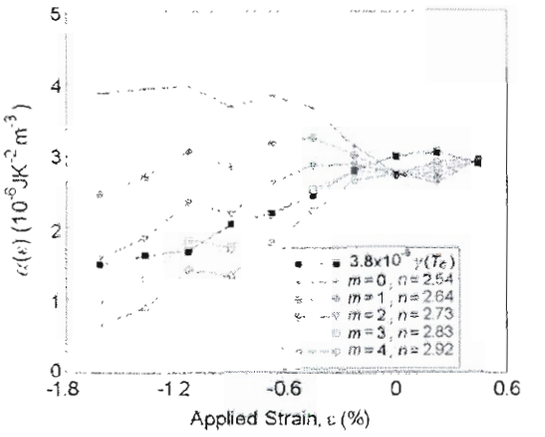

Figure 12. $\alpha(\varepsilon)$ (derived from the critical current data) versus strain generated from the Kramer analysis for the Nb_3Sn strand when $m = 0$, 1, 2, 3 and 4 and the equivalent values of n for best fits are shown. Also shown is $3.8 \times 10^{-9}\gamma(\varepsilon)$ (where $\gamma(\varepsilon)$ has been calculated from $T_c(\varepsilon)$ and the hydrostatic pressure data by Lim *et al* [45]).

on strain, the strong-coupling contribution to $\alpha(\varepsilon)$ only changes by ~5% over the range of strain (or T_C) that we have measured. It is shown below that the change in γ is probably an order of magnitude higher (~50%) than the strong- coupling contribution. Given the large uncertainties in both quantities, we shall concentrate on considering $\gamma(\varepsilon)$: although there has been controversy over the value of γ for Nb_3Sn [44–47], there is now reasonable consensus that 1.176×10^3 J m^{-3} K^{-2} (52.4 mJ K^{-2} mol^{-1}) is a typical value for single crystals [48]. In figure 11, the change in $\gamma(\varepsilon)$ as a function of T_C produced during hydrostatic pressure measurements by Lim *et al* is shown. The data can be approximated by the straight line:

$$\gamma(\varepsilon) = 111T_C(\varepsilon) - 1116. \tag{15}$$

We shall make two bold assumptions. The first is that the relationship between $\gamma(\varepsilon)$ and $T_C(\varepsilon)$ in Nb_3Sn is independent of the type of deformation. Although, it is well known that uniaxial strain has a much larger effect on T_C than hydrostatic strain [49], within the BCS framework, the assumption is equivalent to attributing the effect on T_C of any deformation to changes in electronic rather than phononic properties. The second assumption is that the linearity found in figure 11 for a change in T_C of ~0.4 K holds for the change in T_C of nearly 4 K found in our measurements. These assumptions are borne out of a dearth of $\gamma(\varepsilon)$ data available for high-field superconductors—for example, to our knowledge, there are no heat capacity data on any high-field superconductor as a function of uniaxial strain. The data in figure 7 can be used to calculate a prediction for the uniaxial strain dependence of $\gamma(\varepsilon)$ as shown in figure 12. Also shown in figure 12 is $\alpha(\varepsilon)$ as a function of applied strain derived from linear fits to the data at individual strains in the middle panel of figure 10. To within the accuracy of our measurements and the extrapolation and assumptions used in considering data in the literature, we conclude that for this MJR material $\alpha(\varepsilon)$ and $\gamma(\varepsilon)$ show a similar applied strain dependence when m is in the range 2–3. In figure 12, $\gamma(\varepsilon)$ has been multiplied by 3.8×10^{-9}, so when $m = 2$

$$\alpha(\varepsilon) \approx 3 \times 10^{-3}\mu_0\gamma(\varepsilon). \tag{16}$$

Equations (16) and (11) together imply that $A^* \approx 3 \times 10^{-3}$ (i.e. independent of T and ε) which is consistent with the pinning framework of Dew-Hughes [16] and equation (5).

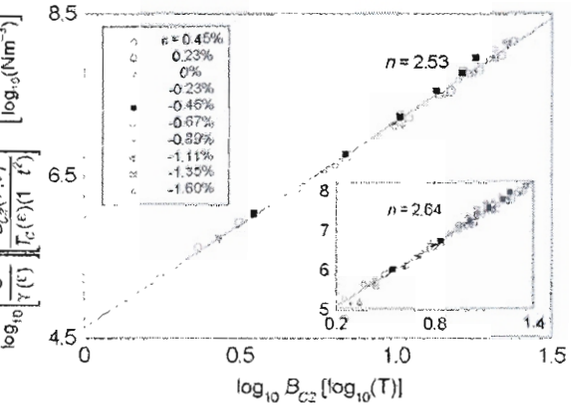

Figure 13. Log–log plot of $\frac{C(T,\varepsilon)}{\gamma(\varepsilon)}\left[\frac{B_{C2}(T,\varepsilon)}{T_c(\varepsilon)(1-t^2)}\right]^2$ versus the upper critical field generated from the Kramer analysis of the data for the Nb_3Sn strand over the technological applied strain range $-0.45\% \leqslant \varepsilon \leqslant 0.45\%$. The inset graph shows the data obtained over the entire range of strain.

In figure 13, we have considered equations (1) and (10) for the technological regime in detail (the entire data set are shown in the inset) and hence explicitly included $\gamma(\varepsilon)$. We again find extremely good linearity consistent with the functional form proposed. Finally, if one notes that the current flow is predominantly in the superconducting layer of the strand and that the layer accounts for about 30% of the total cross-sectional area, the volume pinning force ($F_{P(S/C)}$) within the Nb_3Sn superconducting filaments can be described in terms of superconducting parameters in the form

$$F_{P(S/C)} \approx \frac{1}{100}\frac{B_{C2}^{5/2}(T,\varepsilon)}{(2\pi\Phi_0)^{1/2}\mu_0\kappa^2(T,\varepsilon)}b^{1/2}(1-b)^2. \tag{17}$$

5.2.3. The Ginzburg–Landau parameter. Equation (9) can be used to give expressions for the strain dependence of the

Ginzburg–Landau parameter at $T = 0$ and $T = T_C$:

$$\kappa(0, \varepsilon) = 1.03 \frac{B_{C2}(0)}{\mu_0^{1/2} \gamma^{1/2}(\varepsilon) T_C(\varepsilon)} \left[1 - \frac{1}{5} \left(\frac{2\Delta}{k_B T_C} - 3.53 \right) \right]^{1/2} \tag{18}$$

and [16]

$$\kappa(T_C, \varepsilon) = \kappa(0, \varepsilon) \frac{\upsilon}{2}. \tag{19}$$

For the MJR material, using $\upsilon = 1.374$ gives at zero applied strain $\kappa(0, 0) \sim 45$ and $\kappa(T_C, 0) \sim 31$ which are consistent with typical values in the literature.

5.3. *Technological parameterization of $J_E(B, T, \varepsilon)$*

The values of $\alpha(\varepsilon)$, $T_C(\varepsilon)$ and $B_{C2}(0, \varepsilon)$ in equation (14) can be parameterized using fourth-order polynomial functions [16] where

$$\left.\begin{matrix} \alpha(\varepsilon_I) \\ T_C(\varepsilon_I) \\ B_{C2}(0, \varepsilon_I) \end{matrix}\right\} = c_0 + c_1\varepsilon_I + c_2\varepsilon_I^2 + c_3\varepsilon_I^3 + c_4\varepsilon_I^4 \tag{20}$$

and c_n are constants. We have used a least-squares fit using *Solver* in the *Microsoft Excel* software package to optimize the constants c_n, υ and υ (and chosen to set $p = 1/2$ and $q = 2$—although this constraint is not required). The parameterizations of α, T_C and B_{C2} are described in terms of intrinsic strain ε_I, and the applied strain ε, where $\varepsilon_I = \varepsilon - \varepsilon_M$. This has the effect of setting c_1 to zero and incorporating the degree of freedom in ε_M. Furthermore, the value of ε_M was constrained to be identical for all three parameters without significant loss of accuracy—again this constraint is not required. The accuracy of the parameterization is unaffected by whether the strain-dependent variables are parameterized using applied strain directly or intrinsic strain. Intrinsic strain is more useful since there is evidence that although the spring (material and design) on which the strand is soldered affects the value of ε_M, to a first approximation the intrinsic strain dependence is unaffected [50]. The group in Twente is developing a parameterization of $B_{C2}(\varepsilon)$ based on detailed physical considerations of the affect of strain in three dimensions which may ultimately replace the non-physical polynomial fits used in this work [51]. However, we have not used this parameterization as yet, because in the current standard form, $\partial B_{C2}(\varepsilon)/\partial\varepsilon$ monotonically increases with increasing compression which is not consistent with the data in figure 7.

The constants in tables 1 and 2 together with equations (4) and (14) can be used to generate J_E. Beyond the B–T–ε phase space specified for the coefficients, the parameterization becomes inaccurate. Table 1 gives a parameterization for the Nb_3Sn strand which has been restricted to the phase space of most interest to magnet design engineers. It describes the I_C data obtained to a typical accuracy of $\sim 1\frac{1}{2}$ A. In table 2, equivalent data are presented for Nb_3Al using data generated in previous work [16]. A comparison and interpretation of the c_n coefficients for Nb_3Sn and Nb_3Al are discussed below. Coefficients that parameterize the Nb_3Al and Nb_3Sn data throughout the entire range measured have also been calculated (not shown) in which the accuracy of the parameterization significantly decreased to typically $\sim$6 A.

Table 1. Free parameters in a fourth-order polynomial description of the strain-dependent variables $\alpha(\varepsilon_I)$, $T_C(\varepsilon_I)$ and $B_{C2}(0, \varepsilon_I)$ for Nb_3Sn in terms of intrinsic strain where $\varepsilon_I = \varepsilon - \varepsilon_M$. To convert from engineering critical current density (J_E) to critical current (I_C), one need only multiply all the coefficients for $\alpha(\varepsilon_I)$ by the cross-sectional area (1.96×10^{-7} m^2). Data were fitted for I_C greater than 5 A in the applied strain range $-0.45\% \leqslant \varepsilon \leqslant 0.45\%$, at temperatures 4.2, 6, 8 and 10 K at all fields measured. The remaining constants n, p, q and υ in the parameterization have the values 3.38, $\frac{1}{2}$, 2 and 1.2515 respectively. An Excel spreadsheet showing the use of these coefficients is available at http://www.dur.ac.uk/superconductivity.durham/iterdata.html.

Strain-dependent parameters	$\alpha(\varepsilon_I)$	$B_{c2}(0, \varepsilon_I)$	$T_c(\varepsilon_I)$
ε_{max} (%)	0.2070	0.2070	0.2070
c_0	3.111×10^{-7}	28.10	18.55
c_1	0	0	0
c_2	5.239×10^{-7}	−23.77	−7.451
c_3	9.708×10^{-7}	−11.81	−11.06
c_4	7.286×10^{-7}	3.712	−7.658

Table 2. Free parameters in a fourth-order polynomial description of the strain-dependent variables $\alpha(\varepsilon_I)$, $T_C(\varepsilon_I)$ and $B_{C2}(0, \varepsilon_I)$ for Nb_3Al in terms of intrinsic strain where $\varepsilon_I = \varepsilon - \varepsilon_M$ taken from [16]. To convert from engineering critical current density (J_E) to critical current (I_C), one need only multiply all the coefficients for $\alpha(\varepsilon_I)$ by the cross-sectional area (5.28×10^{-7} m^2). Data were fitted for I_C greater than 5 A in the applied strain range $-0.67\% \leqslant \varepsilon \leqslant 0.67\%$, at temperatures 4.2, 6, 8 and 10 K and at all fields measured. The remaining constants n, p, q and υ in the parameterization have the values 3.1286, $\frac{1}{2}$, 2 and 1.28 respectively. An Excel spreadsheet showing the use of these coefficients is available at http://www.dur.ac.uk/superconductivity.durham/iterdata.html.

Strain-dependent parameters	$\alpha(\varepsilon_I)$	$B_{c2}(0, \varepsilon_I)$	$T_c(\varepsilon_I)$
ε_{max} (%)	0.1389	0.1389	0.1389
c_0	5.357×10^{-7}	24.33	16.24
c_1	0	0	0
c_2	7.068×10^{-8}	−3.124	−1.178
c_3	-1.015×10^{-7}	0.9159	0.1057
c_4	-1.211×10^{-7}	1.839	0.06231

6. Discussion

Despite the enormous academic interest in high-temperature superconductors (HTS), Chevrel phase superconductors and MgB_2, there is no doubt that at present the most important useful materials in the large commercial/technological markets such as MRI body scanners, particle accelerators, fusion coils and high-field research magnets are NbTi and A15 materials (notably doped-Nb_3Sn and Nb_3Al) [52, 53]. J_E in these important materials can be accurately approximated using scaling laws. Nevertheless, it remains to be seen to what degree the scaling laws capture the underlying science. For the Nb_3Sn reported here, there is a significant difference between the two scaling laws for B_{C2} measured resistively and determined as a free parameter from the F_P scaling law (cf figures 4 and 6). There are Sn gradients in these technological strands that lead to distributions in T_C and B_{C2} [54]. In this context, one can interpret the low-B_{C2} values derived from the Kramer plots as characteristic of an average for the filaments or perhaps the local B_{C2} in the region of the pinning sites and the higher values of B_{C2} from the resistive

measurements as characteristic of those parts of the filaments with the highest superconducting critical parameters. One should also consider whether the form for the field dependence of the scaling (i.e. equation (1)) prejudices the fitted values for B_{C2} to below the thermodynamic upper critical field. In light of the strong evidence for the importance of the irreversibility field (B_{irr}) in HTS materials, Chevrel phase [55] and MgB_2 superconductors [56], non-pinning mechanisms such as thermal activation may also play an important role in determining $B_{C2}^{Kramer}(T, \varepsilon)$ in A15 materials. If the resistivity data provides the correct value for B_{C2}, we must consider whether F_P scaling is simply a reasonable approximation of a more general non-scaling law and hence F_P scaling does not accurately describe the mechanism that determines J_E. In this context, the work on HTS materials [57, 58] with high J_E [59, 60] suggests that explicitly including the irreversibility field may help provide an accurate description of J_E. However, despite the continuing improvements in the quality of HTS conductors and the enormous effort directed at concepts such as collective pinning [61], flux creep [62, 63] and the irreversibility field [64, 65] we are far from any clear theoretical consensus on how to parameterize J_E in HTS. In this paper we have ignored the complexities highlighted by HTS work in light of the vast body of experimental data on technologically important low-temperature superconductors in the literature that are accurately described by scaling laws. We have set aside the issue of whether $B_{C2}^{Kramer}(T, \varepsilon)$ should be considered an upper critical field or an irreversibility field and whether there is a significant difference between these fields in Nb_3Sn [66, 67]. Rather, we have focused on how to improve the accuracy and utility of the scaling law for F_P in the technologically important part of B–T–ε phase space (and constrained B_{C2} using equation (4)) since even as a better understanding of high-field superconductors develops, from a magnet engineering perspective the accurate parameterization provided by the proposed scaling framework may be retained within a better understanding of the free parameters—particularly B_{C2}, p and q.

We have made the working assumption that the critical current data can be accurately parameterized using a scaling law given by equation (5). When $m = 0$, and A^* is a constant, the form for F_P is given by the well-known Fietz–Webb scaling law widely used in the literature to describe the field and temperature dependence of J_E for many different superconducting materials. However, to describe the field, temperature and strain dependence of J_E, for the modified jelly-roll data studied here (and for bronze-route Nb_3Sn and Nb_3Al), A^* must vary as a function of strain [14, 15]. Furthermore, $m = 0$ is not really justifiable given that the essence of any pinning mechanism is that the energy of the system is dependent on the spatial distribution of the fluxons within the superconductor and hence any mathematical description of pinning within the Ginzburg–Landau framework must include these energy considerations and hence both B_{C2} and κ [14, 15]. Also $m = 0$ does not give the best fit to the data (cf figure 10). For technological purposes, it is important that the functional form used for F_P is sufficiently general to incorporate the important underlying science and parameterize the data as accurately as possible over as wide a range of magnetic field, temperature and strain. We have considered equation (5) because it is consistent with much of the historical experimental data, many of the theoretical flux pinning models proposed and the more recent $J_E(B, T, \varepsilon)$ data. However, the functional form will have reduced utility either if an unreasonably large range of measurements are required to find the free parameters or if there are so many free (correlated) parameters that the best fits give meaningless constants which are, for example, very sensitive to small changes in the range over which the data are fitted. In the latter context we suggest that the previous data sets for bronze-route Nb_3Sn [14, 15], jelly-roll Nb_3Sn [21, 22] and Nb_3Al [16] can be parameterized making the assumption that $m = 2$ without losing significant accuracy. If we assume that the scaling law has the form of equation (5) where A^* is a constant and that the expression for κ (equation (9)) is valid, then the scaling analysis (figure 10) demonstrates that $m = 2$ provides the best fit. If we have a more limited data set, we find a larger range of m and n values fit the data equally well. Hence we suggest that setting $m = 2$ is a reasonable approach for parameterizing data for technological strands because it eliminates one of the free parameters while retaining an accurate parameterization of available data and hence facilitates interlaboratory comparisons. Over the technological range where $n = 2.53$ (cf figure 13), we note that if we assume $n = 5/2$, A has dimensionless units. Comparison with the Summers relation shows that the proposed scaling law includes an additional factor of $T_C^2(\varepsilon)$—not included in Summer's work. This factor is clearly important for example in trying to understand the affect of radiation on J_E in conjunction with studies where the Sommerfeld constant (γ) [68], resistivity [69] and the critical temperature [70, 71] have been measured as a function of radiation damage. The widespread utility of Summers' form for F_P is consistent with the form proposed for F_P since in principle $T_C^2(\varepsilon)$ (as well as the strong-coupling correction—cf equation (11)) could be incorporated into $\alpha(\varepsilon)$ in equation (10).

In considering the c_n coefficients given in table 1 for Nb_3Sn and in table 2 for Nb_3Al, one can broadly interpret c_0 as the maximum value of the strain-dependent variable when the intrinsic strain is zero and ε_M as the precompression exerted on the filaments as the composite strand cools to cryogenic temperatures. Such simple interpretation is not possible for higher order coefficients because of the simplicity of the polynomial parameterizations and the strong correlations between the $\alpha(\varepsilon_1)$, $T_C(\varepsilon_1)$ and $B_{C2}(0, \varepsilon_1)$ and the constants in the fits. For example, if we parameterize $\alpha(\varepsilon_1)$ for Nb_3Sn over the range $-0.45\% \leqslant \varepsilon \leqslant 0.45\%$, we find a positive value for c_2 consistent with the small minima when $\varepsilon_1 \approx 0$. However, if we parameterize the data over the full strain range, consistent with the broadly inverted parabola shown in figure 12, c_2 is of similar magnitude but changes sign. Despite reservations about any detailed interpretation of c_2, comparing the values of c_2/c_0 in table 1 with those in table 2, we find that they are typically more than a factor 5 higher in Nb_3Sn than in Nb_3Al. Hence in the context of this work, the higher strain sensitivity of J_E in Nb_3Sn occurs because its Sommerfeld constant is more strain sensitive which directly affects α and (consistent with BCS and G-L theory) means that T_C and B_{C2} are more strain sensitive.

Finally, we note that it would help the development of new superconducting strands if the number of measurements

needed to properly parameterize J_E could be reduced. It is known that for a wide range of different Nb_3Sn conductors, the normalized intrinsic strain dependence of T_C can be well approximated by a universal curve [15]. This opens the possibility that one can specify $T_C(\varepsilon)$ with far fewer measurements. Equally, if a larger data base shows that there are other universal relations for example say between $B_{C2}(0, \varepsilon)$ and $T_C(\varepsilon)$ as shown in figure 8, it may become possible to reduce even further the data that are required to specify with reasonable accuracy the $J_E(B, T, \varepsilon)$ surface.

7. Summary and conclusions

Detailed measurements of the critical current density of a modified jelly-roll Nb_3Sn strand have been completed in the applied strain ranges, $-2.15\% \leqslant \varepsilon \leqslant 0.45\%$ for 4.2 K and $-1.6\% \leqslant \varepsilon \leqslant 0.45\%$ above 4.2 K, in the temperature range 4.2 K $\leqslant T \leqslant$ 20 K and the magnetic field range up to 15 T. Scaling laws were found for both F_P and B_{C2}. The F_P data were accurately parameterized using a functional form justified for both strong and weak coupling. The functional form includes a factor $\left[\frac{T_C(\varepsilon)(1-t^2)}{B_{C2}(T,\varepsilon)}\right]^2$, which helps describe the temperature and strain dependence of $\left[\frac{1}{\kappa(T,\varepsilon)}\right]^2$ without the addition of any more free variables.

The proposition in this paper is that for technological purposes, J_E data can be usefully parameterized using

$$F_P = \alpha(\varepsilon)[T_C(\varepsilon)(1-t^2)]^2 \frac{\{B_{C2}(T,\varepsilon)\}^{n-2}}{(2\pi\Phi_0)^{1/2}\mu_0} b^p(1-b)^q \quad (13)$$

and

$$B_{C2}(T, \varepsilon) = B_{C2}(0, \varepsilon)[1 - t^v]. \quad (4)$$

The constants n, p q and v and the strain-dependent variables $\alpha(\varepsilon)$, $T_C(\varepsilon)$ and $B_{C2}(0, \varepsilon)$ have been found for a MJR Nb_3Sn strand and compared to equivalent values for a Nb_3Al strand.

Acknowledgments

We acknowledge support from EPSRC, Oxford Instruments Plc and the ITER programme. Particular thanks are due to D M J Taylor for detailed discussion of the work and the development of the accompanying Excel files. We are also grateful to P Russell for help with the figures; G Teasdale, P Armstrong and P Foley for technical support. One of the authors (SK) was supported by an OI CASE award. Support is also acknowledged from C Forty, N Mitchell, A Portone and E Salpietro.

References

[1] Fietz W A and Webb W W 1969 Hysteresis in superconducting alloys—temperature and field dependence of dislocation pinning in niobium alloys *Phys. Rev.* 178 657
[2] Hampshire R G and Taylor M T 1972 Critical supercurrents and pinning of vortices in commercial Nb-60 at% Ti *J. Phys.* F 2 89
[3] Welch D O 1985 An approximate closed-form expression for the electron-scattering-induced interaction between magnetic flux lines and grain boundaries *IEEE Trans. Magn.* 21 827–30
[4] Dew-Hughes D 1974 Flux pinning mechanisms in type II superconductors *Phil. Mag.* 30 293
[5] Kroeger D M, Easton D S, DasGupta A, Koch C C and Scarbrough J O 1980 The effect of strain upon the scaling law for flux pinning in bronze process Nb_3Sn *J. Appl. Phys.* 51 2184
[6] Ekin J W 1980 Strain scaling law for flux pinning in practical superconductors: part I. Basic relationship and application to Nb_3Sn conductors *Cryogenics* 20 611
[7] Hampshire D P, Jones H and Mitchell E W J 1984 An in-depth characterisation of $(NbTa)_3Sn$ filamentary superconductor *IEEE Trans. Magn.* 21 289
[8] Summers L T, Guinan M W, Miller J R and Hahn P A 1991 A model for the prediction of Nb_3Sn critical current as a function of field, temperature strain and radiation damage *IEEE Trans. Magn.* 27 2041
[9] Specking W, Klemm M, Fluikiger R, Bruzzone P and Ricci M 1991 The effect of static and cyclic axial strain on I_c of cable in conduit NET subcables *IEEE Trans. Magn.* 27 1825–8
[10] Specking W, Kiessel H, Nakajima H, Ando T, Tsuji H, Yamada Y and Nagata M 1993 First results of strain effects on I_C of Nb_3Al cable in conduit fusion superconductors *IEEE Trans. Magn. Appl. Super.* 3 1342
[11] Summers L T, Duenas A R, Karlsen C E, Ozeryansky G M and Gregory E 1991 A characterisation of internal-Sn Nb_3Sn superconductors for use in the proof of principles (POP) coil *IEEE Trans. Magn.* 27 1763
[12] ten Haken B, Godeke A and ten Kate H H J 1999 The strain dependence of the critical properties of Nb_3Sn conductors *J. Appl. Phys.* 85 3247
[13] Martinez A and Duchateau J L 1997 Field and temperature dependencies of critical current on industrial Nb_3Sn *Cryogenics* 37 865
[14] Cheggour N and Hampshire D P 1999 Unifying the strain and temperature scaling laws for the pinning force density in superconducting niobium–tin multifilamentary wires *J. Appl. Phys* 86 552
[15] Cheggour N and Hampshire D P 2002 The unified strain and temperature scaling law for the critical current density of bronze-route Nb_3Sn in high magnetic fields *Cryogenics* 42 299–309
[16] Keys S A, Koizumi N and Hampshire D P 2002 The strain and temperature scaling law for the critical current density of a jelly-roll Nb_3Al strand in high magnetic fields *Supercond. Sci. Technol.* 15 991
[17] Ginzburg V L and Landau L D 1957 On the theory of superconductivity *Zh. Eksp. Teor.* 20 1064
[18] Bardeen J, Cooper L N and Schreiffer J R 1957 Theory of superconductivity *Phys. Rev.* 108 1175
[19] Mitchell N 1999 ITER magnet design and R & D *Fusion Eng. Des.* 46 129
[20] Cheggour N and Hampshire D P 2000 A probe for investigating the effect of magnetic field, temperature and strain on transport critical currents in superconducting wires and tapes *Rev. Sci. Instrum.* 71 4521
[21] Keys S A, Cheggour N and Hampshire D P 1999 The effect of hot isostatic pressing on the strain tolerance of the critical current density found in modified jelly roll Nb_3Sn wires *IEEE Appl. Super.* 9 1447
[22] Taylor D M J, Keys S A and Hampshire D P 2002 Reversible and irreversible effects of strain on the critical current density of a niobium–tin superconducting wire *Cryogenics* 42 109
[23] Ekin J W 1983 Four-dimensional J–B–T–ε critical surface for superconductors *J. Appl. Phys.* 54 303
[24] McKinnell J C, Smathers D B, Siddall M B and O'Larey P M 1995 Improved superconducting critical current density in modified jelly roll Nb_3Sn by the application of niobium (Nb) diffusion barriers *IEEE Trans. Appl. Super.* 5 1768
[25] Keys S and Hampshire D P 2002 Handbook of superconductivity: characterisation of the transport critical current density for conductor applications *Handbook of Superconducting Materials* ed D Cardwell and D Ginley (Bristol: Institute of Physics Publishing)

[26] Walters C R, Davidson I M and Tuck G E 1986 Long sample high sensitivity critical current measurements under strain *Cryogenics* **26** 406
[27] Mathu F and Meijer H C 1982 Some electrical feedthroughs to be used at low temperature *Cryogenics* **22** 428
[28] Friend C M and Hampshire D P 1995 A probe for the measurement of the transport critical current density of superconductors in high magnetic fields and at temperatures between 2 and 150 K *J. Meas. Sci. Technol.* **6** 98
[29] Campbell A M and Evetts J E 1972 Flux vortices and transport currents in type II superconductors *Adv. Phys.* **21** 395
[30] Kramer E J 1973 Scaling laws for flux pinning in hard superconductors *J. Appl. Phys.* **44** 1360
[31] Ekin J W 1979 Strain dependence of the critical current and critical field in multifilamentary Nb_3Sn composites *IEEE Trans. Magn.* **15** 197
[32] Banno N, Takeuchi T, Itoh K, Wada H, Matsumoto H and Tachikawa K 2001 Pinning characteristics of (Nb, Ta)$_3$Sn superconductors produced by Nb/Ta–Sn composite process *IEEE Trans. Appl. Super.* **11** 3696
[33] Cicchelli O, Bottura L, Gilson P and Spadoni M 1995 *IEEE Trans. Appl. Super.* **5** 901
[34] Mitrovic B, Zarate H G and Carbotte J P 1984 The ratio $2\text{Delta}/k_BT_C$ within Eliashberg theory *Phys. Rev.* B **29** 184
[35] Marsiglio F and Carbotte J P 1986 Strong-coupling corrections to Bardeen–Cooper–Schreiffer ratios *Phys. Rev.* B **33** 6141
[36] Moore D F, Zubeck R B, Rowell J M and Beasley M R 1979 Energy gaps of the A-15 superconductors Nb_3Sn, V_3Si, Nb_3Ge measured by tunneling *Phys. Rev.* B **20** 2721
[37] Wilson Paperback M N 1986 *Superconducting Magnets* (Oxford: Oxford University Press)
[38] Abrikosov A A 1957 On the magnetic properties of superconductors of the second group *Sov. Phys. JETP* **5** 1174
[39] Tinkham M 1996 *Introduction to Superconductivity* 2nd edn (Singapore: McGraw-Hill)
[40] Wordenweber R 1999 Mechanism of vortex motion in high-temperature superconductors *Rep. Prog. Phys.* **62** 187
[41] Hampshire D P and Jones H 1987 A detailed investigation of the E–J characteristic and the role of defect motion within the flux-line lattice for high-current-density, high field superconducting compounds with particular reference to data on Nb_3Sn throughout its entire field-temperature phase space *J. Phys.* C **20** 3533
[42] Hampshire D P, Clark A F and Jones H 1989 Flux pinning and scaling laws for superconducting V_3Ga *J. Appl. Phys.* **66** 3160
[43] Kroeger D M, Easton D S, Koch C C and DasGupta A 1980 *Evidence for Microstructural Effects Under Strain in Bronze Process Nb_3Sn* (New York: Plenum)
[44] Orlando T P, McNiff E J, Foner S and Beasley M R 1979 Critical fields, Pauli paramagnetic limiting and material parameters of Nb_3Sn and V_3Si *Phys. Rev.* B **19** 4545
[45] Lim K C, Thompson J D and Webb G W 1983 Electronic density of states and TC in Nb_3Sn under pressure *Phys. Rev.* B **27** 2781
[46] Vieland L J and Wicklund A W 1968 Specific heat of niobium–tin *Phys. Rev.* **166** 424
[47] Stewart G R, Cort B and Webb G W 1981 Specific heat of A15 Nb_3Sn in fields up to 18 Tesla *Phys. Rev.* B **24** 3841
[48] Mitrovic B, Schachinger E and Carbotte J P 1984 Thermodynamics of superconducting Nb_3Al, Nb_3Ge, Nb_3Sn and V_3Ga *Phys. Rev.* B **29** 6187
[49] Welch D O 1980 Alteration of the superconducting properties of A15 compounds and elementary composite superconductors by nonhydrostatic elastic strain *Adv. Cryog. Eng.* **26** 48
[50] Specking W, Duchateau J L and Decool P 1998 First results of strain effects on critical current of Incoloy Jacketed Nb_3Sn CICC's *Proc. 15th Conf. Magn. Techn.* p 1210
[51] Godeke A, ten Haken B and ten Kate H H J 2002 The deviatoric strain description of the critical properties of Nb_3Sn conductors *Physica* C **372–376** 1295
[52] Mitchell N and Salpietro E 2001 ITER R&D: magnets:toroidal field model coil *Fusion Eng. Des.* **55** 171
[53] Seeber B (ed) 1998 *Handbook of Applied Superconductivity* (Bristol: Institute of Physics Publishing)
[54] Lee P J and Larbalestier D C 2001 Compositional and microstructural profiles across Nb_3Sn filaments produced by different fabrication methods *IEEE Trans. Appl. Super.* **11** 3671
[55] Zheng D N, Ramsbottom H D and Hampshire D P 1995 Reversible and irreversible magnetization of the Chevrel phase superconductor $PbMo_6S_8$ *Phys. Rev.* B **52** 12931
[56] Larbalestier D C, Cooley L D, Rikel M O, Polyanskii A A, Jiang J, Cava R J and Haas M 2001 Strongly linked current flow in polycrystalline forms of the superconductor MgB_2 *Nature* **410** 186
[57] Bednorz J G and Muller K A 1986 Possible high T_C superconductivity in the Ba–La–Cu–O system Z. *Phys.* B **64** 189
[58] Wu M K, Ashburn J R, Torng C J, Hor P H, Meng R L, Gao L, Huang Z J, Wang Y Q and Chu C W 1987 Superconductivity at 93 K in a new mixed-phase Y–Ba–Cu–O compound system at ambient pressure *Phys. Rev. Lett.* **58** 908
[59] Heine K, Tenbrink J and Thoner M 1989 High-field critical current densities in $Bi_2Sr_2Ca_1Cu_2O_{8+x}$/Ag wires *Appl. Phys. Lett.* **55** 2441
[60] Larbalestier D C, Gurevitch A, Feldmann D M and Polyanskii A 2001 High-T_C superconducting materials for electric power applications *Nature* **414** 368
[61] Larkin A I and Ovchinnikov Y N 1979 Pinning in type II superconductors *J. Low Temp. Phys.* **34** 409
[62] Feigelman M V, Geshkenbein V B, Larkin A I and Vinokur V M 1989 Theory of collective flux creep *Phys. Rev. Lett.* **63** 2303
[63] Feigelman M V, Geshkenbein V B and Vinokur V M 1991 Flux creep and current relaxation in high-T_C superconductors *Phys. Rev.* B **43** 6263
[64] Brandt E 1995 The flux-line lattice in superconductors *Rep. Prog. Phys.* **58** 1465
[65] Blatter G, Feigelman M V, Geshkenbein V B, Larkin A I and Vinokur V M 1994 Vortices in high-temperature superconductors *Rev. Mod. Phys.* **66** 1125
[66] Suenaga M, Ghosh G, Xu Y and Welch D O 1991 Irreversibility temperature of Nb_3Sn and NbTi *Phys. Rev. Lett.* **66** 1777
[67] Daniel I J and Hampshire D P 2000 Calculations and measurements of the irreversibility field using a vibrating sample magnetometer *Phys. Rev.* B **61** 6982
[68] Hahn P A, Guinan M W, Summers L T and Okada T 1991 Fusion neutron irradiation effects in commercial Nb_3Sn superconductors *J. Nucl. Mater.* **179** 1127–30
[69] Brown B S, Birtcher R C, Kampwirth R T and Blewitt T H 1978 Resistivity and T_c measurements in low temperature irradiated Nb_3Sn and Nb_3Ge *J. Nucl. Mater.* **72** 76
[70] Nolscher C and Saemann-Ischenko G 1985 Superconductivity and crystal and electronic structures in hydrogenated and disordered Nb_3Ge and Nb_3Sn layers with A15 structure *Phys. Rev.* B **32** 1519
[71] Bauer H, Saur E J and Schmeitzer D G 1975 Effect of neutron irradiations on superconducting properties of A-15 compounds undoped and doped with ^{10}B and ^{235}U *J. Low Temp.* **171** 19